THE JOURNAL OF PHYSICAL CHEMISTRY B

ARTICLE

pubs.acs.org/JPCB

Mechanism for the Autophosphorylation of CheA Histidine Kinase: QM/MM Calculations

Ting Shi,[†,§] Yunxiang Lu,[‡] Xinyi Liu,[†] Yingyi Chen,[†] Hualiang Jiang,[§] and Jian Zhang*[,†]

[†]Department of Pathophysiology, Key Laboratory of Cell Differentiation and Apoptosis of Chinese Ministry of Education, Shanghai JiaoTong University School of Medicine, Shanghai 200025, China

[‡]Department of Chemistry, East China University of Science and Technology, Shanghai 200237, China

[§]Drug Discovery and Design Center, State Key Laboratory of Drug Research, Shanghai Institute of Materia Medica, Chinese Academy of Sciences, Shanghai 201203, China

Supporting Information

ABSTRACT:

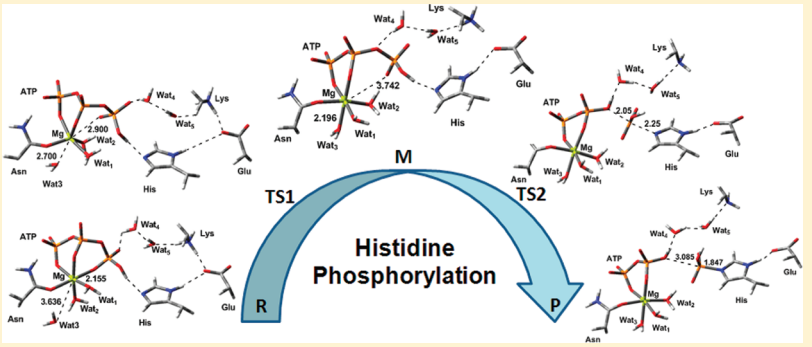

The CheA histidine kinase, a model of TCS (the two-component system), mediates the signal transduction pathway of bacterial chemotaxis via autophosphorylation. Since the TCSs are rarely found in mammalians, they have become attractive targets for the development of new antibiotics. To characterize the autophosphoryl-transfer mechanism of CheA histidine kinase, molecular dynamics simulations combined with quantum mechanics/molecular mechanics calculations were employed on the constructed 3D model of P1−P4−ATP complex. A two-step reaction mechanism was proposed and confirmed by our computations: the autophosphoryl-transfer reaction takes place followed by a rapid and reversible conformational change from ground state to prechemistry state. In addition, a two-dimensional potential energy surface was calculated for autophosphorylation, and the transition state displays an associative character. Moreover, we found Lys48 serves as the catalytic acid to stabilize transition state through a water-mediated proton-transfer pathway, and Glu67 acts as not only a hydrogen bond acceptor but also a structure anchor to modulate the imidazole ring of His45 in the active site. Our findings clearly provide a detailed autophosphoryl-transfer mechanism of CheA histidine kinase and thus are important for discovering new antibiotics.

INTRODUCTION

Two-component signal transduction systems (TCS) are one of the most prevalent means by which bacteria sense, respond, and adapt to changes in their environment or in their intracellular state. In the prototypical TCS pathway, activation of a sensor histidine kinase leads to autophosphorylation on a conserved histidine residue followed by transfer of the phosphoryl group to a cognate response regulator. This regulation by transient phosphorylation of the activity of a protein is a common feature in a wide variety of biological processes, including signal transduction, growth control, and metabolism.[1,2] Because of their complete absence from animals (although present in other eukaryotes such as yeasts[3] and plants[4]), two-component proteins have been targeted for the development of antibacterial drugs.[5−8]

Histidine phosphorylation has been found to be a key feature of bacterial signaling, and histidine kinases transduce information from the extracellular environment to regulate many cellular processes including gene expression, membrane permeability, energy production, and motility.[9−11] As a protein histidine kinase (PHK), CheA functions in the chemotaxis signal transduction pathway of many bacteria and archaea and has been widely investigated by detailed structural and biochemical analysis.[12−17] The central region of CheA is a histidine kinase module composed of a four-helix bundle dimerization domain formed from the parallel association of two up−down helices, each linked to an ATP-binding catalytic domain that contains the kinase active site. All necessary elements for histidine phosphorylation are found in the phosphor-transfer (P1) and kinase (P4)

Received: April 28, 2011
Revised: September 1, 2011
Published: September 12, 2011

dx.doi.org/10.1021/jp203968d | J. Phys. Chem. B 2011, 115, 11895–11901

domains of the five-domain CheA protein.[18] ATP binding takes place in domain P4, and the autophosphorylation site is located in domain P1. Conserved residues in the P4 domain bind ATP in a pocket that optimally positions the γ-phosphoryl for transfer to a specific histidine (His45 in *Thermotoga maritime* and His48 in *Salmonella typhimurium*) on the N-terminal P1 domain.[13,14] In addition, domain P2 is a specific domain for recognizing CheY and assists transfer of the phosphoryl group, domain P3 mediates dimer formation, and domain P5 is responsible for binding and regulatory interactions with CheW and chemotaxis receptor protein.

A fundamental question regarding the histidine kinase is its catalytic mechanism; i.e., how does P1 domain of CheA catalyze the transfer of γ-phosphoryl group of ATP to the phosphor-accepting histidine? How does ATP contribute to CheA phosphorylation? Which residue may play an important role in the autophosphorylation? Despite extensive experimental studies,[19−22] some detailed mechanistic issues including the nature of the transition state have not yet been fully addressed. To our best knowledge, no theoretical study with quantum mechanics/molecular mechanics (QM/MM) methods has been carried out to study the phosphorylation mechanism of histidine kinase. Here we focus on the P1−P4−ATP complex,[23] a constructed CheA histidine kinase system described in our previous paper, to study the mechanism of the autophosphorylation.

Our previous work[23] with the molecular dynamics (MD) simulation on the construct 3D model of P1−P4−ATP complex indicated that ATP is not only a phosphoryl group donor but also an activator for CheA phosphorylation. These simulation results are in agreement with the findings of mutagenesis experiments.[24] In the present study, the model structure in aqueous solution obtained from the MD simulation was further optimized using ab initio QM/MM methods to investigate the mechanism of the autophosphorylation of CheA histidine kinase. A two-step reaction mechanism is proposed and confirmed by our computational results. Two-dimensional potential energy surfaces were calculated to better understand the reaction pathway. Also, the key stable states and transition states as well as activation energy barrier were obtained. Moreover, Lys48 and Glu67 are shown to play an essential role in both ATP binding and CheA catalytic process. This computational prediction was verified by additional experimental mutagenesis[15,25] and kinetic analysis.[19] Findings from this work should be important to better understand the enzymatic mechanism of CheA, to elucidate the specific role of some key residues, and to provide theoretical understanding of its reaction specificity and information for designing antimicrobial drugs.

EXPERIMENTAL METHODS

3D Model of P1−P4−ATP Complex. A 3D model of the *T. maritime* P1 was generated by means of homology modeling using the X-ray structure of the *S. typhimurium* P1 (1I5N)[25] as a template, since the alignment analysis showed that *S. typhimurium* P1 shares ~60% full sequence similarity with *T. maritime* P1, especially on the consistency of the active site around His45 (89% similarity in nine residues), suggesting that *S. typhimurium* P1 could provide accurate structural information to model *T. maritime* P1. After modeling, the root-mean-square deviation (rmsd) for the backbone atoms between the template and the modeled *T. maritime* P1 is below 1.2, revealing structural confidence for the modeling of *T. maritime* P1. The ligand−protein docking approach was used to construct a 3D model of P4−ATP complex based on the structure of P4−ADPCP complex (1I58).[13] Finally, the protein−protein docking program, 3D-DOCK, was applied to construct the 3D model of P1−P4−ATP complex (Supporting Information Figure S1). In detail, the 3D structure of P1 has a cylinder-like geometry with a diameter of ~18 Å, which is very close to the shape of the binding site of P4 in its open state. Also kinetic experimental data provide significant information to constrain the distance between His45 and ATP. Therefore, both of them may facilitate the confident match between P1 and P4 in protein−protein docking, as discussed by Wodak and Ritchie.[26,27] In addition, 3D-DOCK algorithm performs an energy minimization and removal of steric clash on the side chains of the interface after docking, also leading to the better recurrence of P1−P4−ATP complex conformation. The detailed processes have been described in previous work.[23]

MD Simulation. The GROMACS program[28] with the GROMOS96 force field[29] was used to perform the MD simulations on the P1−P4−ATP complex. The molecular topology files for ATP were generated by the program PRODRG. The partial atomic charges of ATP were determined by using the CHelpG method implemented in the Gaussian03 program[30] at the level of the HF/6-31G*. A total of 15 Na^+ ions were included to maintain the electrical neutrality of the total system, and then the P1−P4−ATP model was solvated with the simple point charge (SPC) water model. To maintain the system at a constant temperature of 300 K, the Berendsen thermostat was applied using a coupling time of 0.1 ps. The pressure was maintained by coupling to a reference pressure of 1 bar. A coupling time of 1.0 ps was used for the simulation in bulk water. The P1−P4−ATP complex including protein, ATP, and sodium ions as well as water molecules was encompassed with a rectangular parallelepiped solvent box. The dimensions of the box (approximately $8.9 \times 8.3 \times 7.2$ nm^3) ensured that no atom within the kinase−ATP active site complex is less than 8 Å from any face of the box. Finally, a 4 ns equilibration MD simulation was carried out on the P1−P4−ATP system, and the rmsd for the C^α atoms of P1−P4−ATP is shown in the Supporting Information Figure S3A.

QM/MM Calculation. QM/MM calculations were performed by using a two-layered ONIOM method encoded in the Gaussian03 program. The ONIOM method[31−35] is a hybrid computational method developed by Morokuma and co-workers that allows different levels of theory to be applied to different parts of a molecular system.

The final snapshot from the equilibration obtained by using the AMBER Parm99 force field was further optimized at the ONIOM (B3LYP/6-31G*:Amber) level. McCammon et al.[36] carried out classic QM/MM calculations on the phosphorylation reaction of PKA with different QM/MM partition schemes, in which a QM subsystem with the triphosphate arm of ATP and with the whole ATP are both approximately consistent with the experimental estimation. Their result has shown that the triphosphate arm of ATP in QM may be adequate and efficient in the study of catalytic mechanism and the difference between the theoretical and the experimental energies might not always benefit from large QM due to additional approximations for a large QM/MM boundary. Herein, we used the triphosphate arm of ATP in the study of catalytic reaction of histidine kinase. The QM region includes the α, β, γ-phosphate group of fully unprotonated ATP, five water molecules including three coordinated water molecules, Mg^{2+} ion, the protonated terminal group of His45, the methyleneammonium group ($-CH_2-N^{\zeta}H^+_3$) of

Lys48, and the anionic carboxymethyl group ($-CH_2-COO^-$) of Glu67 for a total of 40 atoms, which brings the total charge of the QM system to -1 (the total system remained neutral). The QM region was calculated by using the density functional theory with the B3LYP exchange-correlation functional and 6-31G* basis set. The remainder of the system (MM region) was treated by using the AMBER Parm99 force field. A total of 5687 atoms were included for the QM/MM calculations. The electrostatic interactions between the QM and MM regions were calculated by using the electronic embedding method, which treats the polarization of the QM region by the MM region with scaled partial atomic charges of MM atoms, and the response of the QM region with the Merz−Singh−Kollman scheme for charge fitting so as to produce the changing partial charges of the QM atoms. The protonation state of residue in a protein is dependent on both its type and local environment, which is generally estimated by pK_a in computational biology. Moreover, the pK_a values of the ionizable groups can also change upon ligand binding, which has been observed in a couple of systems.[37−39] In the study of histidine kinase, considering that the local environment of the imidazole group of His45, only carboxyl negative group ($-COO^-$) of Glu67, γ-phosphate negative group ($-PO^-$) of ATP, and O atom of Wat5 are around it within the range of 3.5 Å (Figure 3 and Figure S2 in the Supporting Information), then the free energy of protonated His45 with positive charge is much better than that of deprotonated His45, which may lead to more stable conformation of such groups through electrostatic interactions with each other. Thus, higher pK_a of His45 in the microenvironment of P1−P4−ATP could be indicated, and double-protonated His45 was supported by the evaluation of the PROPKA program[40] (http://propka.ki.ku.dk/). The result shows that the pK_a of His45 is 5.0 and 8.26 before and after ATP binding, indicating double-protonated His45 may play an important role at the beginning of the reaction. Therefore, we started this autophosphoryl-transfer reaction with protonated His45.

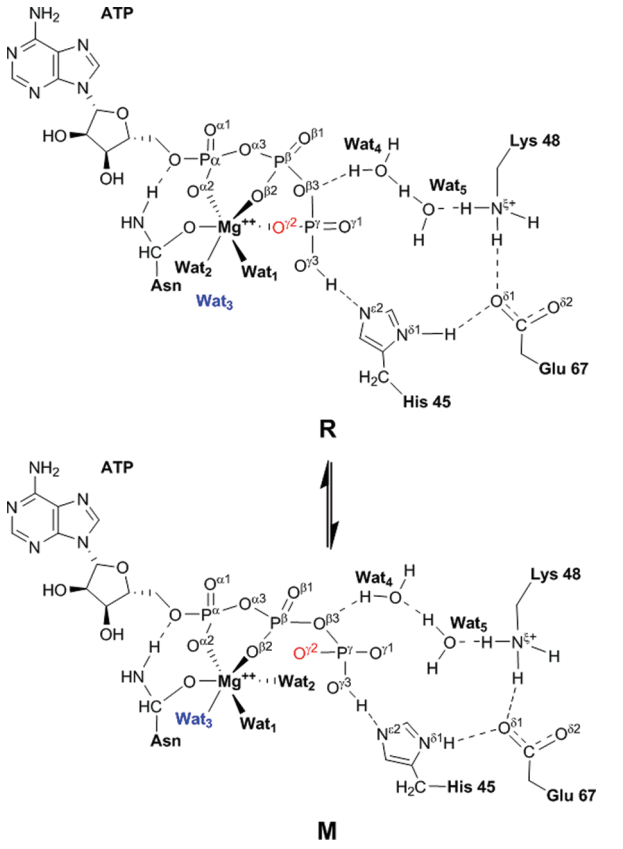

Figure 1. Conformational change between **R** and **M**.

RESULTS AND DISCUSSION

Two-Step Reaction Mechanism. The final typical conformation from the equilibration obtained by MD simulations was further fully optimized at the ONIOM (B3LYP/6-31G*: Amber) level. A stable ground state structure **R** was located, indicating the importance of the conformation in the catalytic process of

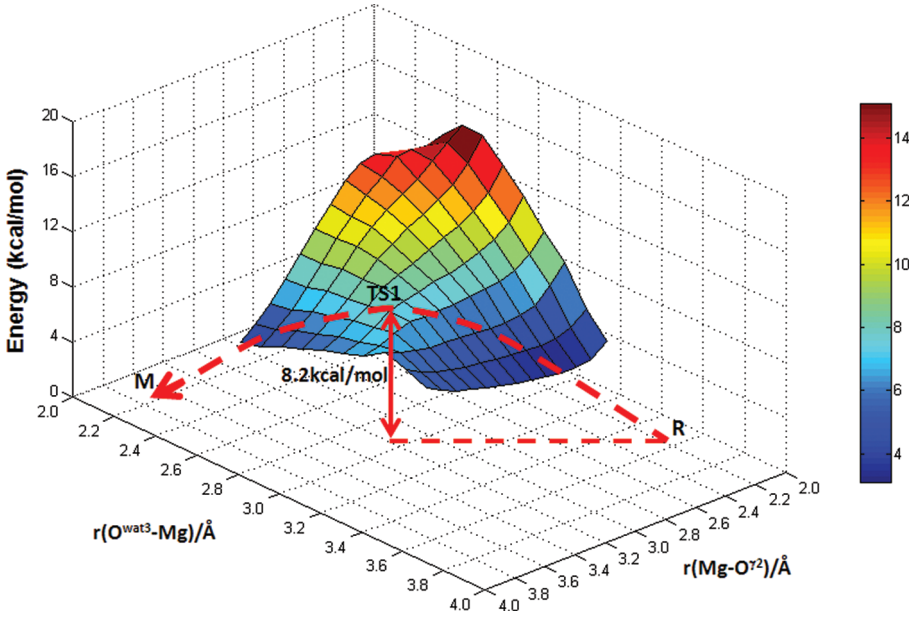

Figure 2. Two-dimensional potential energy surface defining the distances of $r(Mg-O^{\gamma 2})$ and $r(O^{Wat3}-Mg)$ as the reaction coordinates.

dx.doi.org/10.1021/jp203968d |J. Phys. Chem. B 2011, 115, 11895–11901

histidine kinase. To evaluate the reliability of **R**, the Protein Data Bank was searched, and we found that the conformation of **R** is a typical prerequisite for enzyme catalysis in proteins, such as AMP-activated protein kinase (PDB ID code: 2 V9J) and P_{II} signal transduction protein (PDB ID code: 2ZXW), in which both O^{β} and O^{γ} atoms of ATP bind to Mg^{2+} ion (shown in the Supporting Information Figure S4). Furthermore, the major difference of **R** for the reaction center from the initial structure obtained by MD simulation is that a proton from the $N^{\varepsilon 2}$ of His45 imidazole is captured by the $O^{\gamma 3}$ atom of ATP. The deprotonation of imidazole occurred automatically because of the nucleophilic character of γ-phosphoryl of ATP. In detail, the **R** structure shows that in the active site Mg^{2+} ion octahedrally coordinates with the $O^{\alpha 2}$, $O^{\beta 2}$, and $O^{\gamma 2}$ atoms of ATP, the O^{δ} atom of Asn, and two oxygen atoms from two water molecules. However, the arrangement of reactive atoms in this structure is unfavorable for the phosphorylation reaction, since the γ-phosphate group of ATP is stuck to the binding of Mg^{2+} ion. Therefore we proposed a prechemistry state, designated as **M**, in which a local conformational change occurs in the active site (Supporting Information Figure S5A): the triphosphate arm of ATP slightly extends, and the distance between the $O^{\gamma 3}$ atom of the γ-phosphate group and the $N^{\varepsilon 2}$ atom of His45, viz., $r(O^{\gamma 3}-N^{\varepsilon 2})$, is closer from 2.807 to 2.730 Å, the $O^{\gamma 2}$ atom of ATP is replaced by an oxygen atom of water molecule bound to the catalytic Mg^{2+} ion, and the γ-phosphate group keeps away from the Mg^{2+} ion approaching the His45. This change can then facilitate the phosphor-transfer reaction. Meanwhile, the Mg^{2+} ion is far away from the $O^{\gamma 2}$ atom of the γ-phosphate group from 2.155 to 3.636 Å and moves toward the amide group in the side chain of Asn161. As the effect of induced fit, the amide group of Asn161 rotates to ~31° in a clockwise direction, leading to an adequate distance at 2.085 Å between the O^{δ} atom of Asn161 and the Mg^{2+} ion. Other residues of the catalytic environment have no obvious change observed from the **R** conformation to the **M** conformation. Fortunately, we easily obtained the prechemistry structure **M** by ONIOM optimization, which is in great agreement with our proposal.

The conformational change between **R** and **M** is shown in Figure 1 and similar conformational change between ground state and prechemistry state has also been reported by Lin.[41] Compared with the stability of these two complexes, we find that **M** is less stable than **R** by 1.3 kcal/mol. Furthermore, a two-dimensional potential energy surface was calculated at the ONIOM (B3LYP/6-31G*:Amber) level to understand the conformational change. This calculated potential energy surface by defining the distances of $r(Mg-O^{\gamma 2})$ and $r(O^{Wat3}-Mg)$ as the reaction coordinates is presented in Figure 2, and the key active-site structures along the reaction path, including **R**, **TS1**, and **M**, are illustrated in Figure 3. The distance of $r(Mg-O^{\gamma 2})$ is found to be 2.155 Å in the optimized structure **R** and 3.636 Å in the optimized product **M**, and the distance of $r(O^{Wat3}-Mg)$ is 3.742 Å in **R** and 2.196 Å in **M**; **TS1** is located at $r(Mg-O^{\gamma 2})$ = 2.90 Å and $r(O^{Wat3}-Mg)$ = 2.70 Å, and we think the steric demand induced by inserting the oxygen atom of Wat2 into the $Mg-O^{\gamma 2}$ bond will be responsible for the large bond length of 2.90 Å. Furthermore, the calculated potential energy barrier is $\Delta E\ddagger$ = 8.2 kcal/mol.

These results indicated that the conformational change between ground state **R** and prechemistry state **M** is easily proceeding according to such a low activation energy barrier (8.2 kcal/mol), which is in good agreement with their energy

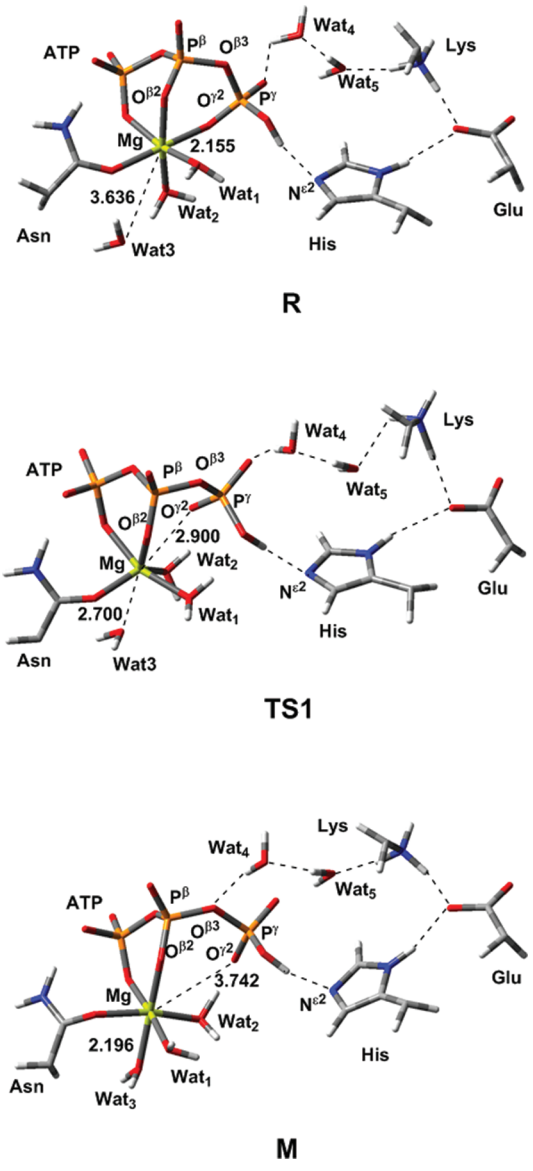

Figure 3. Optimized structure of **R**, **M**, and **TS1**; black dashed lines represent hydrogen bonds or key bond distances (in Å) of the conformational change between **R** and **M**. For clarity, only the atoms around the reaction center are included.

difference (6.97 kcal/mol) calculated with Amber force field used in classical MD (Supporting Information Figure S5B). Also it can be suggested from these results that this reaction step is rapid and reversible. This conformational change is believed to be an essential initial step for the success of the autophosphorylation. Therefore, we proposed a two-step reaction mechanism, where (1) a prechemistry state **M** is formed through a rapid and reversible conformational change, and then (2) the autophosphoryl-transfer reaction moves on.

Our results are in great agreement with Stock' postulation.[42] His kinetic data support a mechanism of CheA regulation that involves perturbation of an equilibrium between two forms of substrate−kinase complexes, which are consistent with **R** and **M**. Also, it is consistent with Stewart's publication[22] where in the presence of Mg^{2+}, the ATP binding mechanism is a rapid, reversible step that enhanced the overall affinity of the complex.

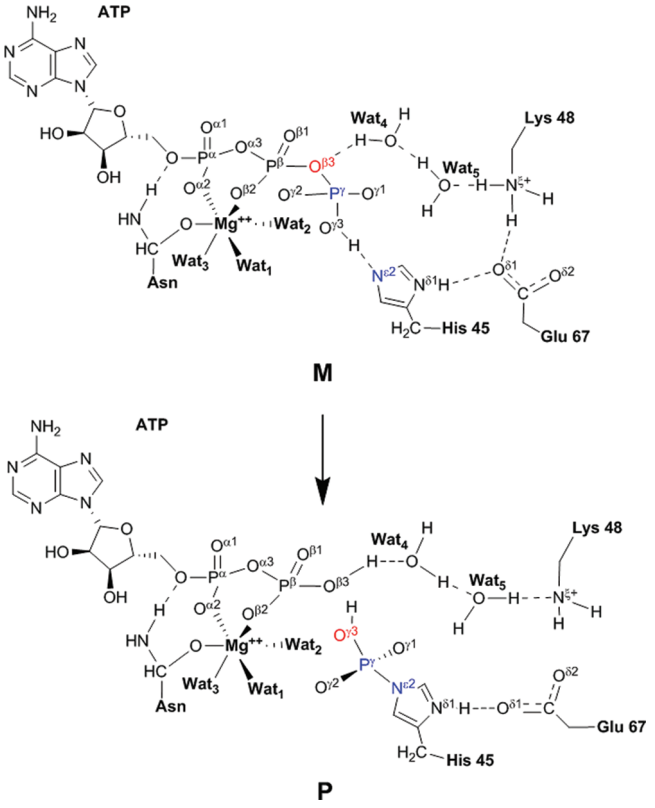

Figure 4. Proposed mechanism of autophosphoryl-transfer reaction.

Furthermore, the γ-phosphate group of ATP in prechemistry state **M** keeps away from the Mg^{2+} ion and approaches the $N^{\varepsilon 2}$ atom of His45, indicating the regulation role of ATP in connecting P1 with P4 domain. More importantly, the autophosphoryl-transfer reaction in such a two-step reaction will have a lower activation energy barrier than the single-step process and therefore improves the catalytic proficiency.

Autophosphoryl-Transfer Reaction Mechanism. The autophosphoryl-transfer reaction mechanism was also investigated by using a two-dimensional potential energy surface with the ONIOM (B3LYP/6-31G*:Amber) method by defining the distances of $r(N^{\varepsilon 2}-P^{\gamma})$ and $r(P^{\gamma}-O^{\beta 3})$ as the reaction coordinates. Since the formation of the $N^{\varepsilon 2}-P^{\gamma}$ bond represents the nucleophilic attack process, the breaking of the $P^{\gamma}-O^{\beta 3}$ bond describes the dissociative process. The proposed mechanism is presented in Figure 4. The distance of $r(P^{\gamma}-O^{\beta 3})$ is found to be 1.649 Å in the optimized structure **M** and finally enlarged to 3.085 Å in the optimized product **P**, and the distance of $r(N^{\varepsilon 2}-P^{\gamma})$ is initially 3.804 Å in **M** and reduced to 1.847 Å in **P**. Furthermore, **TS2** is located at $r(P^{\gamma}-O^{\beta 3})$ = 2.05 Å and $r(N^{\varepsilon 2}-P^{\gamma})$ = 2.25 Å. The autophosphorylation is proposed to be the rate-determining step with the activation barrier of 27.8 kcal/mol. We think the energy barrier might be reduced when different computational methods or/and indispensable solvent effect are considered. The optimized structures of **M**, **P**, and **TS2** with only high-level atoms are shown in Figure 5, and the obtained two-dimensional potential energy surface is presented in Figure 6.

Along the reaction path, as the $N^{\varepsilon 2}$ of His45 imidazole draws closer to the P^{γ} of ATP, a hydrogen bond between $O^{\gamma 3}$ and $N^{\varepsilon 2}$ weakens gradually, until it breaks, while a proton transfer

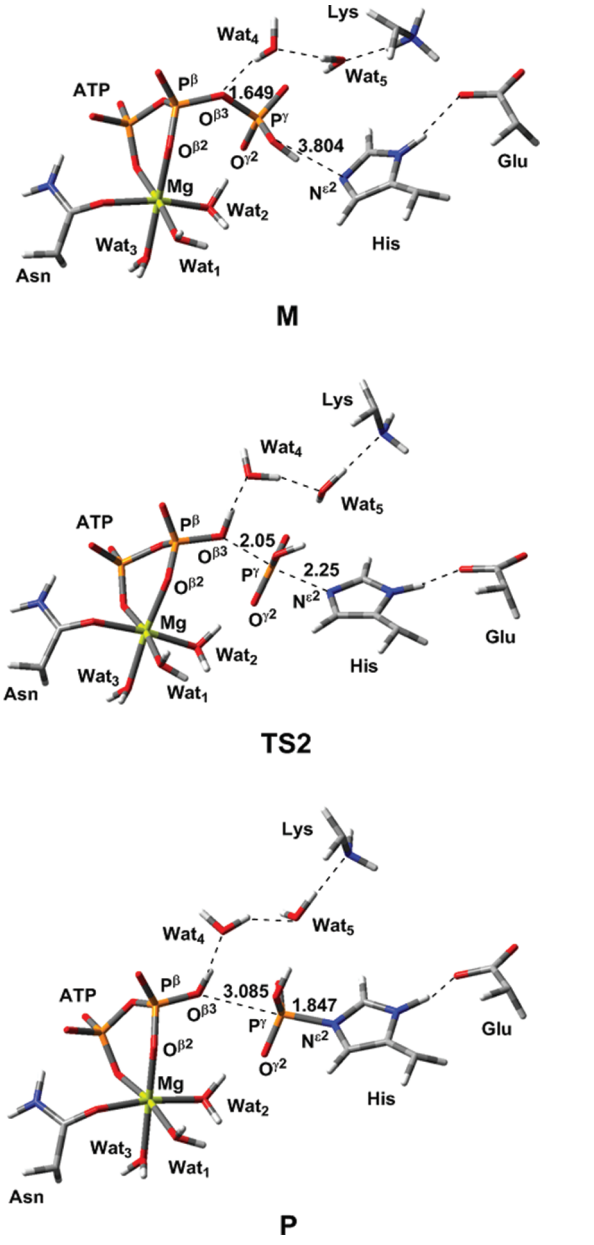

Figure 5. Optimized structures of **M**, **P**, and **TS2**; black dashed lines represent hydrogen bonds or key bond distances (in Å) of autophosphoryl-transfer reaction. For clarity, only the atoms around the reaction center are included.

automatically proceeds from Lys48 to the $O^{\beta 3}$ atom of ATP via two water molecules (Wat4 and Wat5), followed by the breaking of the $P^{\gamma}-O^{\beta 3}$ bond, because of the strong nucleophilic character of the $O^{\beta 3}$ of ATP. The hydrogen bond contributes to the near-attack reactive conformation, and the proton transfer stabilizes the **TS2** through a water-mediated proton-transfer pathway. It is found that the γ-phosphate ($-P^{\gamma}O_3$) of **TS2** is pushed closer to the leaving ADP group (2.05 Å) than the entering substrate imidazole group (2.25 Å) and turned to be in a plane. This structure clearly demonstrates that the $N^{\varepsilon 2}-P^{\gamma}$ bond is partially formed and the $P^{\gamma}-O^{\beta 3}$ bond is partially broken. In one word, we suggest that the autophosphoryl-transfer reaction catalyzed by histidine kinase mainly takes place with an associative mechanism.

dx.doi.org/10.1021/jp203968d |J. Phys. Chem. B 2011, 115, 11895–11901

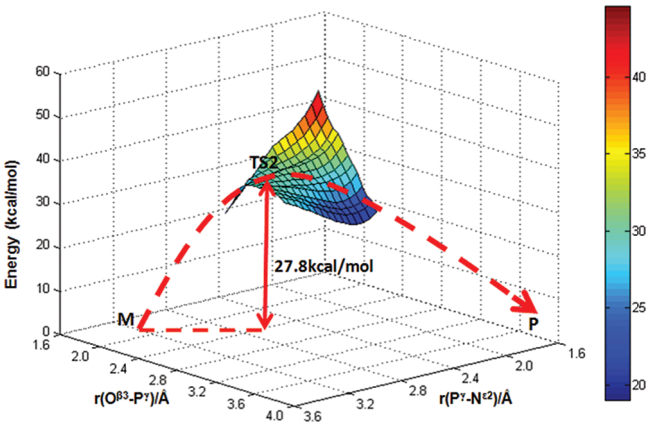

Figure 6. Two-dimensional potential energy surface defining the distances of $r(N^{\varepsilon 2}-P^{\gamma})$ and $r(P^{\gamma}-O^{\beta 3})$ as the reaction coordinates.

In addition, it should be pointed out that **P** is less stable than **M** by 6.3 kcal/mol, suggesting that the reversible reaction will be more easily achieved with an energy barrier of 21.5 kcal/mol. As we know, the phosphorylated histidine residue His∼P might not be stable enough, since the next phosphorylation between His∼P and a conserved aspartate residue will occur rapidly. Our results are in accord with this consensus.

Role of Key Residues. Lys48 is a highly conserved residue in histidine kinase. We proposed that Lys48 may directly participate in the reaction by transfer of one of its protons to the γ-phosphate of ATP for stabilizing the transition state. However, the distance between the $N^{\zeta+}$ of Lys48 and the P^{γ} of ATP in the optimized prechemistry structure (**M**) is 6.34 Å. We investigated their interactions and surrounding environment and found that two water molecules could penetrate the active site and bridge these two residues, and then a water-mediated proton-transfer pathway is proposed to facilitate the autophosphorylation. Our calculations confirmed that Lys48 serves as the catalytic acid to provide the proton to γ-phosphate group through a water-mediated proton-transfer pathway. Experimental mutagenesis[15] verified the role of Lys48.

Besides Lys48, Glu67 is another important residue in the active site of histidine kinase. Mourey[25] suggested that Glu67 may act as a hydrogen bond acceptor for the phosphor-accepting histidine. Our calculations support this proposal. We found that the $O^{\delta 1}$ atom of Glu67 always maintains a hydrogen bond with the $N^{\delta 1}$ atom of His45 in the whole reaction process. It should be pointed out that the bond distance between $N^{\delta 1}$ and $O^{\delta 1}$ decreases from 3.09 Å in **R**, to 3.01 Å in **M**, to 2.54 Å in **P**. Moreover, Glu67 most strongly stabilizes the reagent and intermediate structure by electrostatic interaction with Lys48; the average bond distance in them between $N^{\zeta+}$ of Lys48 and $O^{\delta 1}$ of Glu67 is 2.66 Å, although this hydrogen bond is lost in the transition state and product. Taken together, we think Glu67 acts as not only a hydrogen bond acceptor from Lys48 and His45 but also a structure anchor to modulate the imidazole ring of His45 in the active site. This conclusion is consistent with previous publication.[15]

CONCLUSIONS

The two-component system (TCS) signal transduction is a predominant signaling system mediated by histidine kinase in bacteria, and TCSs are rarely found in mammalians. Therefore these enzymes hold great interest as attractive targets for the development of new antibiotics.

Based on the molecular dynamics (MD) simulations with our constructed 3D model complex, further fully optimizations have been performed by the ONIOM method. A prechemistry state **M** was obtained, and compared with **R**, **M** has a better facilitative effect on the phosphor-transfer reaction, although **M** is less stable than **R** by 1.3 kcal/mol. A two-dimensional potential energy surface was calculated by defining the distances of $r(Mg-O^{\gamma 2})$ and $r(O^{Wat3}-Mg)$ as the reaction coordinates, and the calculated potential energy barrier is $\Delta E\ddagger$ = 8.2 kcal/mol. A two-step reaction mechanism is proposed and confirmed by our computational results: a prechemistry state **M** is formed through a rapid and reversible conformational change, and then the autophosphoryl-transfer reaction moves on.

Another potential energy surface for autophosphorylation was also calculated with the ONIOM method, and this reaction is proposed to be the rate-determining step with the activation barrier of 27.8 kcal/mol. The reversible reaction was found to be more easily achieved by 21.5 kcal/mol, suggesting the phosphorylated histidine residue His∼P might not be stable enough. In addition, the transition state displayed an associative character.

Lys48 serves as the catalytic acid to provide the proton to γ-phosphate group through a water-mediated proton-transfer pathway, and Glu67 acts as not only a hydrogen bond acceptor from Lys48 and His45 but also a structure anchor to modulate the imidazole ring of His45 in the active site. These computational predictions were verified by additional experimental mutagenesis and kinetic analysis. These results provide a detailed autophosphoryl-transfer mechanism of CheA histidine kinase, revealing that the key residues around the active site may be primarily used to rationally design competitive inhibitor against the ATP-dependent phosphotransfer, and therefore will provide theoretical understanding for discovering new antibiotics.

ASSOCIATED CONTENT

Supporting Information. Constructed 3D model of P1−P4−ATP complex (Figure S1); key residues around the active site of P1−P4−ATP complex (Figure S2); rmsd of C^{α} atoms in P1−P4−ATP complex and heavy atoms in the active site of P1−P4−ATP complex relative to the initial structure versus simulation time (Figure S3), respectively; binding environment of O^{β} and O^{γ} atoms of ATP binding to Mg^{2+} ion in AMP-activated protein kinase (PDB ID code: 2 V9J) and O^{α}, O^{β}, and O^{γ} atoms of ATP binding to Mg^{2+} ion in P_{II} signal transduction protein (PDB ID code: 2ZXW) (Figure S4); comparative view of catalytic environments between the **R** conformation and the **M** conformation (Figure S5). This material is available free of charge via the Internet at http://pubs.acs.org.

AUTHOR INFORMATION

Corresponding Author
*E-mail: jian.zhang@sjtu.edu.cn.

ACKNOWLEDGMENT

This work was supported in part by grants from the National Basic Research Program of China (973 Program) (2011CB504001), the National Natural Science Foundation of China (21002062), the Innovative Research Team of Shanghai Municipal Education

Commission, the Program for Professor of Special Appointment (Eastern Scholar) at Shanghai Institutions of Higher Learning, and the Shanghai PuJiang Program (10PJ406800).

REFERENCES

(1) Galperin, M. Y. *BMC Microbiol.* **2005**, *5*, 35.
(2) Gao, R.; Mack, T. R.; Stock, A. M. *Trends Biochem. Sci.* **2007**, *32*, 225–234.
(3) Kruppa, M.; Calderone, R. *FEMS Yeast Res.* **2006**, *6*, 149–159.
(4) Mizuno, T. *Biosci., Biotechnol., Biochem.* **2005**, *69*, 2263–2276.
(5) Stephenson, K.; Hoch, J. A. *Curr. Med. Chem.* **2004**, *11*, 765–773.
(6) Marra, A. *Drugs R. D.* **2006**, *7*, 1–16.
(7) Watanabe, T.; Okada, A.; Gotoh, Y.; Utsumi, R. *Adv. Exp. Med. Biol.* **2008**, *631*, 229–236.
(8) Gotoh, Y.; Eguchi, Y.; Watanabe, T.; Okamoto, S.; Doi, A.; Utsumi, R. *Curr. Opin. Microbiol.* **2010**, *13*, 232–239.
(9) Hanks, S. K.; Quinn, A. M.; Hunter, T. *Science* **1988**, *241*, 42–52.
(10) Parkinson, J. S.; Kofoid, E. C. *Annu. Rev. Genet.* **1992**, *26*, 71–112.
(11) Stock, A. M.; Robinson, V. L.; Goudreau, P. N. *Annu. Rev. Biochem.* **2000**, *69*, 183–215.
(12) Bilwes, A. M.; Alex, L. A.; Crane, B. R.; Simon, M. I. *Cell* **1999**, *96*, 131–141.
(13) Bilwes, A. M.; Quezada, C. M.; Croal, L. R.; Crane, B. R.; Simon, M. I. *Nat. Struct. Biol.* **2001**, *8*, 353–360.
(14) Quezada, C. M.; Gradinaru, C.; Simon, M. I.; Bilwes, A. M.; Crane, B. R. *J. Mol. Biol.* **2004**, *341*, 1283–1294.
(15) Quezada, C. M.; Hamel, D. J.; Gradinaru, C.; Bilwes, A. M.; Dahlquist, F. W.; Crane, B. R.; Simon, M. I. *J. Biol. Chem.* **2005**, *280*, 30581–30585.
(16) Scott, K. A.; Porter, S. L.; Bagg, E. A.; Hamer, R.; Hill, J. L.; Wilkinson, D. A.; Armitage, J. P. *Mol. Microbiol.* **2010**, *76*, 318–330.
(17) Gao, R.; Stock, A. M. *Annu. Rev. Microbiol.* **2009**, *63*, 133–154.
(18) Hess, J. F.; Oosawa, K.; Kaplan, N.; Simon, M. I. *Cell* **1988**, *53*, 79–87.
(19) Eaton, A. K.; Stewart, R. C. *Biochemistry* **2010**, *49*, 5799–5809.
(20) Bhatnagar, J.; Borbat, P. P.; Pollard, A. M.; Bilwes, A. M.; Freed, J. H.; Crane, B. R. *Biochemistry* **2010**, *49*, 3824–3841.
(21) Gloor, S. L.; Falke, J. J. *Biochemistry* **2009**, *48*, 3631–3644.
(22) Stewart, R. C. *Biochemistry* **2005**, *44*, 4375–4385.
(23) Zhang, J.; Xu, Y.; Shen, J.; Luo, X.; Chen, J.; Chen, K.; Zhu, W.; Jiang, H. *J. Am. Chem. Soc.* **2005**, *127*, 11709–11719.
(24) Marina, A.; Mott, C.; Auyzenberg, A. *J. Biol. Chem.* **2001**, *276*, 41182–41190.
(25) Mourey, L.; Da Re., S. *J. Biol. Chem.* **2001**, *276*, 31074–31082.
(26) Wodak, S. J.; Mendez, R. *Curr. Opin. Struct. Biol.* **2004**, *14*, 242–249.
(27) Ritchie, D. W. *Curr. Protein Pept. Sci.* **2008**, *9*, 1–15.
(28) Van Der Spoel, D.; Lindahl, E.; Hess, B.; Groenhof, G.; Mark, A. E.; Berendsen, H. J. *J. Comput. Chem.* **2005**, *26*, 1701–1718.
(29) Schüttelkopf, A. W.; van Aalten, D. M. *Acta. Crystallogr., Sect. D: Biol. Crystallogr.* **2004**, *60*, 1355–1363.
(30) Frisch, M. J.; Trucks, G. W.; Schlegel, H. B.; Scuseria, G. E.; Robb, M. A.; Cheeseman, J. R.; Zakrzewski, V. G.; Montgomery, J. A., Jr.; Stratmann, R. E.; Burant, J. C.; et al. *Gaussian 03*, rev. B.03; Gaussian, Inc.: Pittsburgh, PA, 2003.
(31) Svensson, M.; Humbel, S.; Froese, R. D. J.; Matsubara, T.; Sieber, S.; Morokuma, K. *J. Phys. Chem.* **1996**, *100*, 19357–19363.
(32) Kuno, M.; Hannongbua, S.; Morokuma, K. *Chem. Phys. Lett.* **2003**, *380*, 456–463.
(33) Svensson, M.; Humbel, S; Morokuma, K. *J. Chem. Phys.* **1996**, *105*, 3654–3661.
(34) Vreven, T.; Mennucci, B.; da Silva, C. O.; Morokuma, K.; Tomasi, J. *J. Chem. Phys.* **2001**, *115*, 62–72.
(35) Vreven, T; Morokuma, K; Farkas, O.; Schlegel, H. B.; Frisch, M. J. *J. Comput. Chem.* **2003**, *24*, 760–769.
(36) Cheng, Y; Zhang, Y; McCammon, J. A. *J. Am. Chem. Soc.* **2005**, *127*, 1553–1562.
(37) Trylska, J; Antosiewicz, J; Geller, M; Hodge, C. N.; Klabe, R. M.; Head, M. S.; Gilson, M. K. *Protein Sci.* **1999**, *8*, 180–195.
(38) Alexov, E. *Proteins* **2004**, *56*, 572–584.
(39) Czodrowski, P.; Sotriffer, C. A.; Klebe, G. *J. Mol. Biol.* **2007**, *367*, 1347–1356.
(40) Olsson, M. H. M.; Søndergaard, C. R.; Rostkowski, M.; Jensen, J. H. *J. Chem. Theory Comput.* **2011**, *7*, 525–537.
(41) Lin, P.; Batra, V. K.; Pedersen, L. C.; Beard, W. A.; Wilson, S. H.; Pedersen, L. G. *Proc. Natl. Acad. Sci. U.S.A.* **2008**, *105*, 5670–5674.
(42) Levit, M. N.; Liu, Y.; Stock, J. B. *Biochemistry* **1999**, *38*, 6651–6658.